Detailed Chemical Kinetics for Thermal Decomposition of Low Molecular Weight-Methyl Esters Generated by Using Biodiesel Fuel

Article *in* Environmental Progress & Sustainable Energy · January 2016

DOI: 10.1002/ep.12309

CITATIONS
2

READS
32

4 authors, including:

Phan Quang Thang
Vietnam Academy of Science and Technology
5 PUBLICATIONS **6** CITATIONS
SEE PROFILE

Nguyen Quang Trung
Vietnam Academy of Science and Technology
24 PUBLICATIONS **29** CITATIONS
SEE PROFILE

AIChE

Detailed Chemical Kinetics for Thermal Decomposition of Low Molecular Weight-Methyl Esters Generated by Using Biodiesel Fuel

Phan Quang Thang,[a,b] Yasuaki Maeda,[c] Nguyen Quang Trung,[b] and Norimichi Takenaka[a]

[a]Department of Applied Chemistry, Graduate School of Engineering, Osaka Prefecture University, Sakai-Shi, Osaka 599-8531, Japan; dw105013@edu.osakafu-.ac.jp (for correspondence)

[b]Institute of Environmental Technology (IET), Vietnam Academy of Science and Technology (VAST), Hanoi, Vietnam

[c]Research Organization for University–Community Collaborations, Osaka Prefecture University, Osaka 599-8531, Japan

Published online 00 Month 2016 in Wiley Online Library (wileyonlinelibrary.com). DOI 10.1002/ep.12309

Low molecular weight-methyl ester (LMW-ME), which was reported in our previous study [1], was generated by the use of biodiesel fuel (BDF) with a diesel power generator. In this article, the detailed chemical kinetics for the thermal decomposition of LMW-MEs was investigated at atmospheric pressure and a temperature range of 773 to 973 K. Six standards of LMW-MEs were used for thermal decomposition in a continuous flow reactor. The kinetic data, such as reaction orders, activation energies, and rate constants, were then calculated. The reaction orders and activation energies of the thermal decomposition reactions of C_4, C_5, C_6, C_7, C_8, and C_9 were 1.13, 0.96, 1.17, 0.80, 0.99, 0.84, and 312.04, 117.37, 87.29, 62.94, 74.80, 75.79 kJ mol^{-1}, respectively. The decomposition of LMW-MEs with higher carbon numbers was faster than those with smaller carbon numbers, except for C_8. The C_4 methyl ester was stable and abundant in the product of the decomposition as well as in the exhausted gas from the engine combustion using BDF. This kinetic data will be applied to modeling study on BDF decomposition and engine technologies to mitigate toxic emissions from BDF combustion. © 2016 American Institute of Chemical Engineers Environ Prog, 00: 000–000, 2016

Keywords: low molecular weight-methyl ester, chemical kinetics, thermal decomposition, continuous flow reactor

INTRODUCTION

Biodiesel fuels (BDFs) are derived by transesterification from a variety of bioresources, such as animal fats, catfish oil, vegetable oils, waste cooking oil, and some types of seed oils (rape, palm, *Jatropha curcas*, rubber, *Pongamia pinnata*, etc.). BDFs are complex mixtures composed mainly of five saturated and unsaturated methyl esters: methyl palmitate ($C_{17}H_{34}O_2$), methyl stearate ($C_{19}H_{36}O_2$), methyl oleate ($C_{19}H_{34}O_2$), methyl linoleate ($C_{19}H_{32}O_2$), and methyl linolenate ($C_{19}H_{30}O_2$).

BDF is a well-known renewable alternative for conventional diesel fuel and can be used without any specific modification of diesel engines. Emissions from biodiesel utilization have been interested and characterized. It was determined that the combustion of BDF from diesel engines resulted in lower emission of particulate matter (PM), CO and unburned hydrocarbons. However, BDF usage was also known to increase NOx, carbonyl compounds [2,3], ozone [4,5], and low-molecular weight methyl esters (LMW-MEs) with high toxicity [1]. LMW-MEs have one carbon-carbon double bond at the end of the alkyl chain $C_nH_{2n-2}O_2$ ($n = 4-9$). The concentration of this LMW-ME group increases as the BDF blend ratio increases. In BDF, some components have at least one double bond at the C_{10} position, such as methyl palmitoleate ($C_{17}H_{32}O_2$), methyl oleate ($C_{19}H_{36}O_2$), methyl linoleate ($C_{19}H_{34}O_2$), and methyl linolenate ($C_{19}H_{32}O_2$). Under thermal cracking, cleavage will preferentially occur at the bonds adjacent to the double bond; thus, the C_9 and C_{11} positions will be cleaved first. A carbon chain with a methyl ester radical will be produced by the smaller carbon number methyl ester, which starts at C_9 [1]. The structures and physical properties of LMW-MEs are shown in Table 1 [6]. The carbon chain without the methyl ester radical will be produced alkanes and alkenes. C_4 and C_5 in biodiesel fuel exhausted gas (BFEG) were also detected in the study by Ratcliff *et al.* (2010) [7]. Their results show that the peak area of C_4 was higher than that of C_5. These results are consistent with the results of our previous study; however, Ratcliff *et al.* did not provide a detailed explanation or report their concentrations. C_4 through C_{10} have been observed in the thermal decomposition of methyl decanoate ($C_{11}H_{22}O_2$) [8], whereas C_4 through C_7 have been detected in the oxidation of methyl decanoate, which has been proposed as a possible BDF surrogate [9]. Pedersen *et al.* [10] conducted the oxidation of rapeseed BDF at 823 K and observed LMW-MEs, such as C_4, C_5, C_7, and C_8, of which C_4 was a significant product.

Numerous kinetic studies of BDFs, including oxidations of BDF blend surrogates [8,9,11], small methyl esters [12], soybean and rapeseed BDF [13], and thermal decompositions of soybean BDF [14] and methyl decanoate [8,15], have been conducted either experimentally or theoretically by using computational modeling. To investigate these kinetic studies, the following laboratory experimental

Additional Supporting Information may be found in the online version of this article.

Table 1. Structures and physical properties of the LMW-ME group.

Structure	Name	Formula	Molar weight (g mol^{-1})	Boiling point (K)	Vapor pressure at 298 K
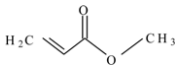	Methyl 2-propenoate (Methyl acrylate)	$C_4H_6O_2$ ($C_2H_3COOCH_3$)	86	353	65
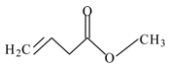	Methyl 3-butenoate	$C_5H_8O_2$ ($C_3H_5COOCH_3$)	100	363	57.29
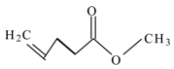	Methyl 4-pentenoate	$C_6H_{10}O_2$ ($C_4H_7COOCH_3$)	114	398-400	44
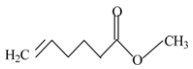	Methyl 5-hexenoate	$C_7H_{12}O_2$ ($C_5H_9COOCH_3$)	128	430	4.62
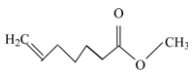	Methyl 6-heptenoate	$C_8H_{14}O_2$ ($C_6H_{11}COOCH_3$)	142	439.9	1.75
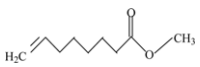	Methyl 7-octenoate	$C_9H_{16}O_2$ ($C_7H_{13}COOCH_3$)	156	462.2	0.58

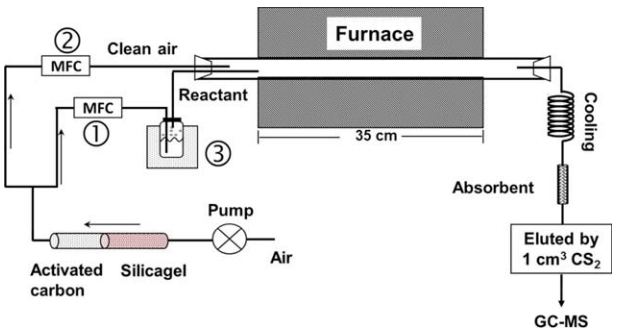

Figure 1. Schematic of the continuous flow reactor system. ① Mass flow controller (MFC) to control reactant flow into the reaction tube. ② MFC to control clean air into the reaction tube for dilution and changing residence time. ③ Thermostat solution is kept at constant temperature. [Color figure can be viewed in the online issue, which is available at **wileyonlinelibrary.com**.]

systems were used; (1) A jet-stirred reactor, which is a type of ideal continuously stirred tank reactor, is mainly used to study the oxidation and pyrolysis of hydrocarbons and oxygenated fuels [16]. This method was applied in the kinetic studies of BDF [13,17–19]; (2) a flow reactor method was applied to investigate the detailed chemical kinetics of thermal cracking [20,21]; (3) finally, a shock tube method was used to study pyrolysis and oxidation [22–24]. In order to calculate the kinetics studies of methyl esters, thermogravimetric analysis (TGA) is commonly applied, which is based on weight loss data at different heating rates [25–27].

As described in our previous study, LMW-MEs which were generated from power engine combustion using waste cooking oil BDF were toxic compounds. In order to understand the hazardous compound emission as LMW-ME, we should identify the kinetic and mechanism of LMW-ME formation resulting from thermal cracking processes. However, the studies of the kinetics and mechanisms of the LMW-MEs are not available. This study presents experimental results of the thermal decomposition of LMW-MEs. The weight loss of LMW-MEs could be observed and the rate constants, reaction orders and activation energies were then calculated from the experimental data.

EXPERIMENT AND METHODOLOGY

Continuous Flow Reactor System

The method of continuous flow reactor systems has been described in several studies [20,28,29], and the thermal decompositions were performed in an isothermal flow quartz reactor at atmospheric pressure. Figure 1 shows the schematic diagram of the experimental system. The quartz tube had an inner diameter of 2.5 cm and a tubular reactor of 35 cm. Both sides of the quartz tube were sealed by silicon rubber caps. The tubular reactor corresponding to a volume of 171.8 cm^3 was placed in a tube in an electric furnace (purchased from As One Co., Ltd., model TMF-300N). The middle portion of the quartz tube was heated in the furnace; therefore, to disperse the temperature around the quartz reaction tube, copper foil was used to wrap the outside of the quartz reaction tube. The temperature distribution of the tube under each reaction temperature was measured by a thermometer (TM-947SD, LT Lutron Co. Ltd.) and the results are shown in Figure 2. The maximum temperature was found in the middle of the tube. Ambient air was treated with silica gel and activated carbon, and then divided into two lines. The first line passed through a reactant solution, which was placed in a glass vaporizer to generate a reactant gas. The concentration of the reactant gas depended on the flow rate and temperature of the thermostat. Table 2 shows the experimental conditions and the concentration of each reactant. The initial concentration of each LMW-ME was determined by the same flow rate without heating. These concentrations did not change in all experiments for the individual LMW-ME. The second line in Figure 1 was a dilution gas which was introduced directly into the quartz tube reactor. The residence time in the tubular reactor was altered by changing the flow rate of this line. Every flow stream was controlled by a mass flow controller which was calibrated by a soap bubble flow meter. After thermal decomposition, sample gas was passed through a stainless steel coil to decrease the temperature before introducing to an absorbent (Carbopack B). The absorbent was then eluted by 1 cm^3 of CS_2 for 1 h. Finally, 1 mm^3 of eluent was injected into a gas chromatograph-mass

spectrometer (GC-MS, Agilent 5975) to analyze the LMW-ME species. Further information on LMW-ME detection and re-used absorbent were described in the Supporting Information of our previous work [1].

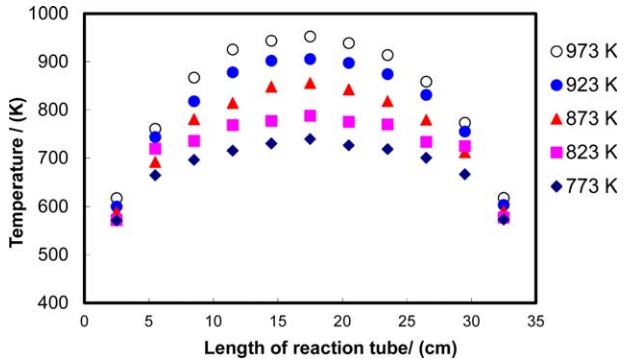

Figure 2. Temperature profile of the tubular reactor in the flow reactor system. [Color figure can be viewed in the online issue, which is available at **wileyonlinelibrary.com**.]

Reagents

LMW-ME standard solutions, C_4, C_5, C_6, and C_8, were purchased from Sigma-Aldrich. C_7 was purchased from Tokyo Chemical Industry Co., Ltd. A reagent-grade CS_2 solvent was purchased from Wako Co., Ltd. C_9 was synthesized by the method described by Yun *et al.* [30]. Briefly, a solution of octenoic acid (1 cm^3) in methanol (24 cm^3) was added to sulfuric acid (0.3 cm^3, 5.7 mmol) at room temperature, and the mixture was refluxed for 24 h by Soxhlet extraction. The mixture was then concentrated using an evaporator, and the residual solution

Table 2. Temperature, flow rate, and corresponding concentration of each LMW-ME.

Compound	Temperature (K)	Reactant flow (mL min^{-1})	Generated reactants rate (μg min^{-1})
C4	253	5	157.18
C5	258	5	4.93
C6	268	10	2.04
C7	278	50	3.88
C8	285	50	4.85
C9	293	50	6.74

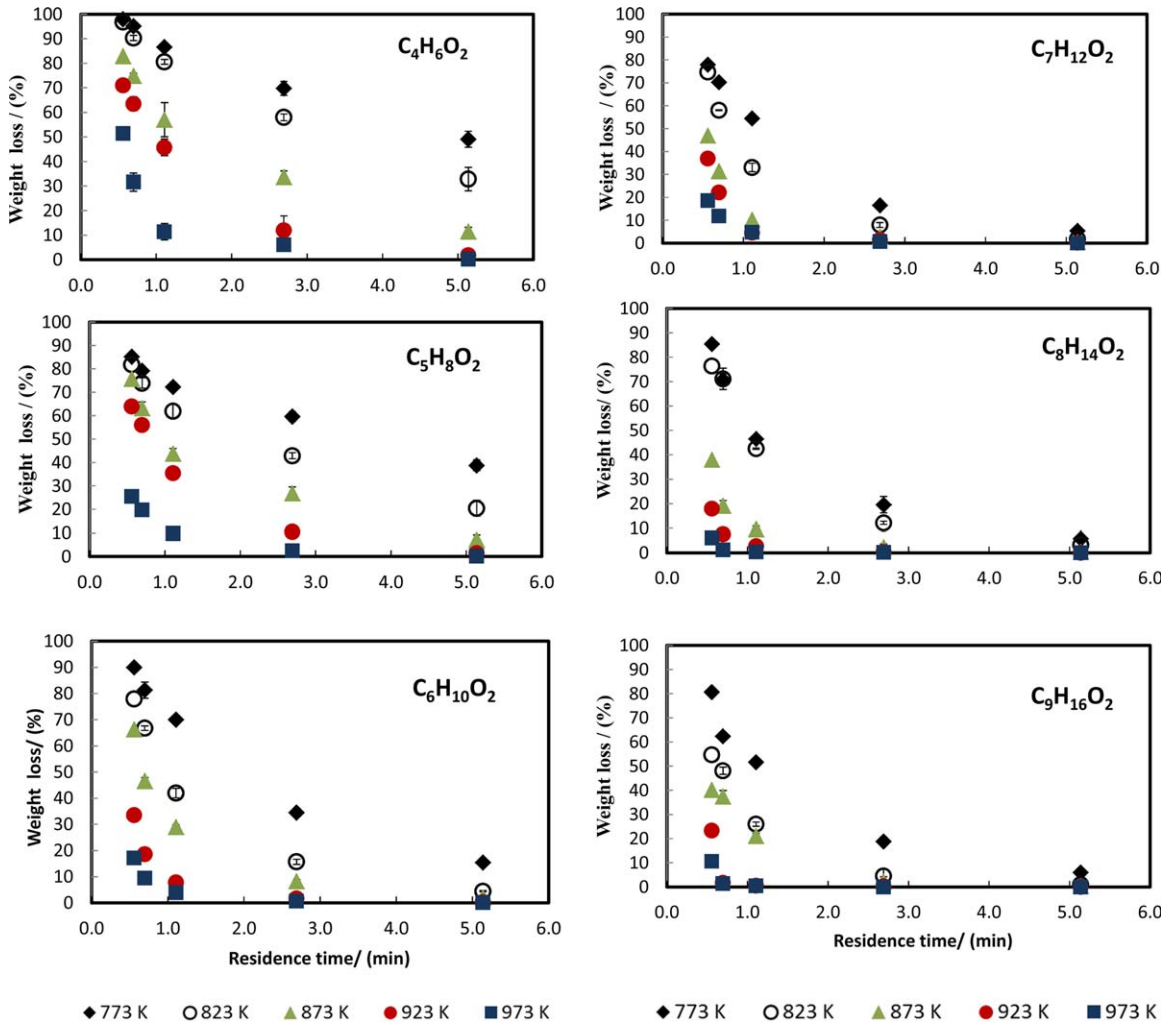

Figure 3. Percentage of residual reactants during the time of thermal decomposition. The percentage of weight loss expressed as the residual reactant in % compared with initial concentration. [Color figure can be viewed in the online issue, which is available at **wileyonlinelibrary.com**.]

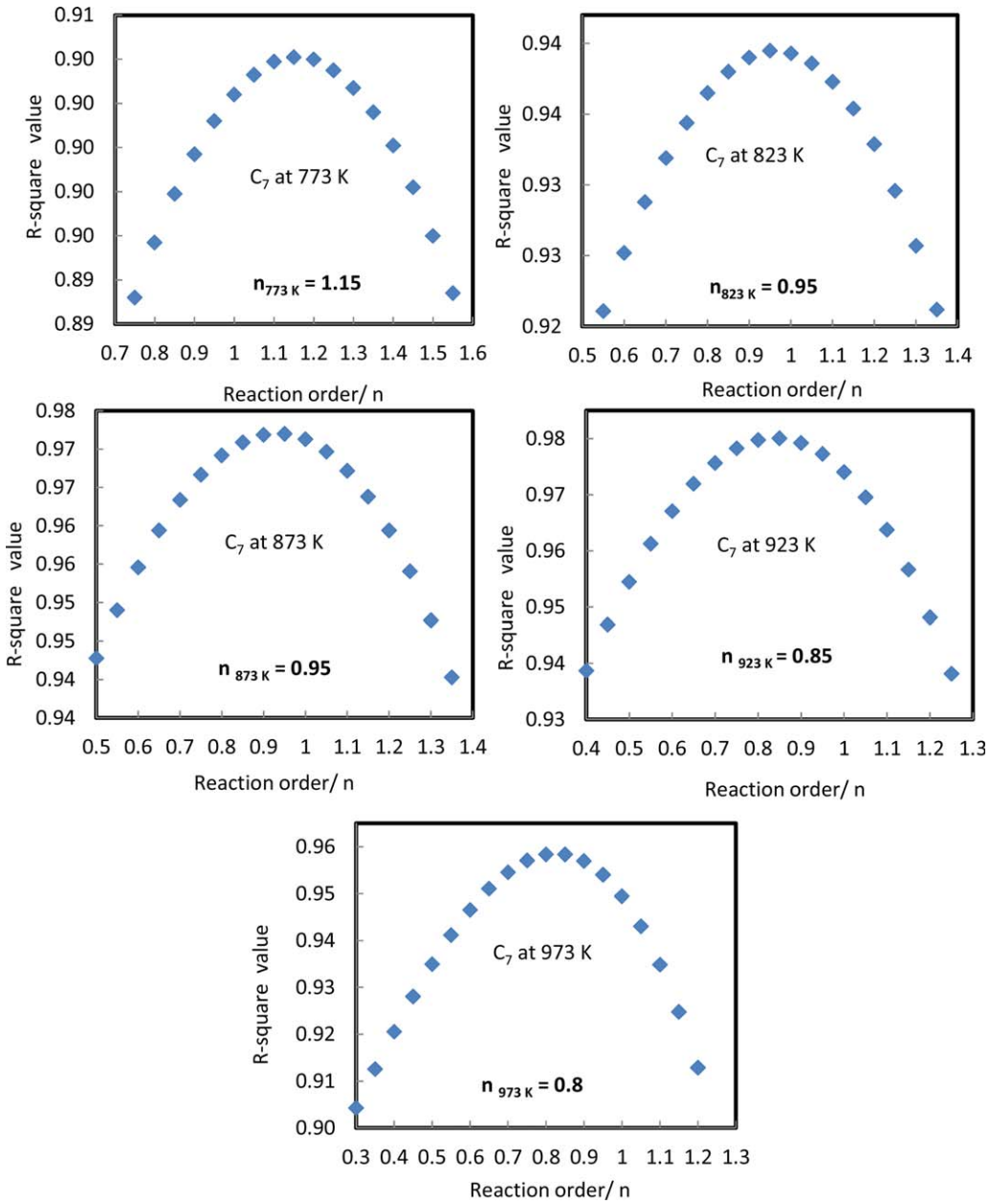

Figure 4. An example for the determination of the reaction order of C_7 decomposition. The reaction order is detected when R^2 reached a maximum (R^2 value was determined by plotting the concentration of the residual reactant *versus* the residence time). [Color figure can be viewed in the online issue, which is available at **wileyonlinelibrary.com**.]

Table 3. Kinetic data of LMW-ME thermal decomposition.

LMW-ME	N	Reaction order ($n \pm$ SD)	$E_a \pm$ SD (kJ/mole)	ln$A \pm$ SD
C4	5	1.13 ± 0.47	312.04 ± 47.60	42.64 ± 6.77
C5	5	0.96 ± 0.24	117.37 ± 15.13	16.32 ± 2.15
C6	5	1.17 ± 0.31	87.29 ± 23.69	12.08 ± 3.37
C7	5	0.80 ± 0.13	62.94 ± 12.55	9.53 ± 1.78
C8	5	0.99 ± 0.18	74.80 ± 10.09	10.88 ± 1.44
C9	4	0.84 ± 0.21	75.79 ± 11.92	11.77 ± 1.74

SD, standard deviation; N, number of data.

(approximate 1 cm^3) was dissolved in ethyl ether (5 cm^3). The solution was washed with saturated aqueous $NaHCO_3$ solution (3 cm^3 × three times), and the remaining water was removed by activated Na_2SO_4. The solution was concentrated by an N_2 stream to vaporize ethyl ether and methanol. Finally, the solution of methyl-7-octenoate was produced in 95% yield.

RESULTS AND DISCUSSIONS

Determination of Reaction Orders, Rate Constants, and Activation Energies

The continuous flow reactor method was applied in this study because LMW-ME groups are easy to vaporize at room

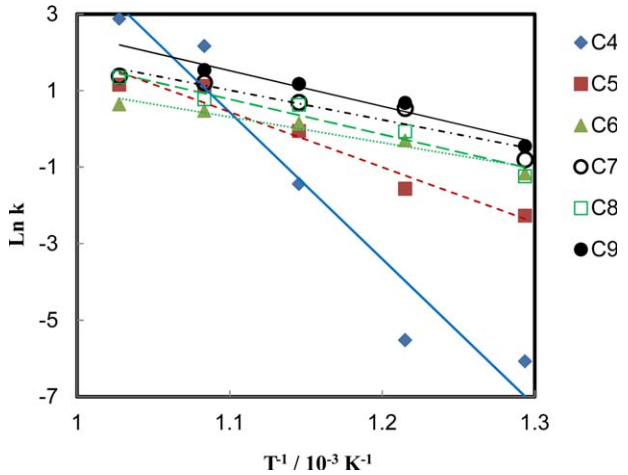

Figure 5. Arrhenius plots. The rate constant of C_4 was extremely large and gradually decreased with increasing carbon number. [Color figure can be viewed in the online issue, which is available at **wileyonlinelibrary.com**.]

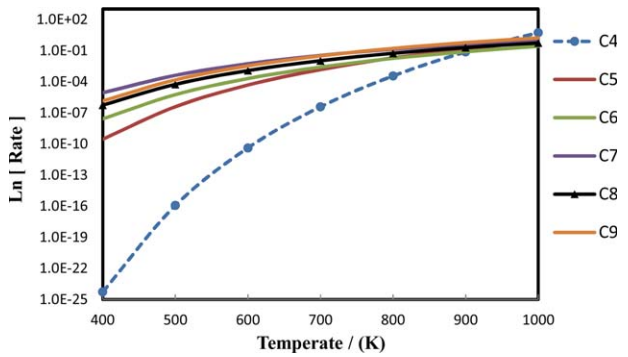

Figure 6. Correlation between LMW-ME decomposition rate and temperature. [Color figure can be viewed in the online issue, which is available at **wileyonlinelibrary.com**.]

temperature and atmospheric pressure. The temperature ranged from 773 to 973 K in this kinetic study. Archambault and Billaud [31] also studied the pyrolysis of rapeseed oil BDF in the same temperature range using a flow reactor method. This temperature range is suitable because of the incomplete thermal decomposition of LMW-MEs. Under each temperature condition, the residence times were varied by changing the flow rate of the dilution gas. The reactants, dilution flow, total flow rate, and residence time of the decomposition are shown in Table S1 of the Supporting Information. The initial concentrations of individual LMW-MEs were also different at different residence times because of the changing flow rate in the tubular reactor. The initial concentration of individual LMW-ME depending on total flow is shown in Table S2 of the Supporting Information. Figure 3 shows that the concentrations of the reactants were decreased by thermal decomposition, depending on the temperature and residence time. The weight loss concentrations were expressed in % for consistency and ease of comparison, thus each value was normalized to its initial concentration. Basically, the higher carbon number methyl esters decomposed faster than the lower carbon number methyl esters. That means the decomposition reaction preferentially

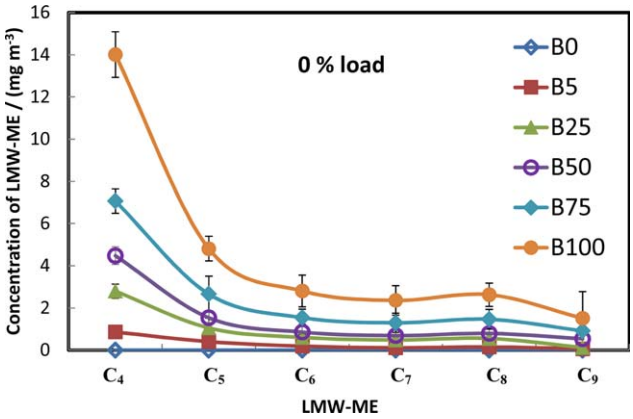

Figure 7. Concentration of individual LW-MEs in the exhausted gas from an engine power generator using BDF. Experimental conditions: 0% load (idling mode) and variation of blended fuel ratio from B0 (0% BDF in volume) to B100 (100% BDF in volume). [Color figure can be viewed in the online issue, which is available at **wileyonlinelibrary.com**.]

occurred with the long chain methyl esters. Thus, C_9 was quickly cleaved even at 723 K within 0.29 min and decomposed completely at 973 K with a residence time of 2.91 min.

The reaction orders cannot be determined from Figure 3, except in the case where n equals 1. Because the initial concentration for each residence time was different, the reaction order was determined by fitting the n value from 0.1 to 2 in Eq. (1). The left side of Eq. (1) was calculated from the initial concentration, the concentration at each residence time, and each n value. Then, by plotting the left side of Eq. (1) *versus* the residence time (t), the reaction order was determined from the graph with the highest R^2 value, where the slope of this graph was equal to the rate constant (k). Finally, the activation energy, E_a, was determined by the Arrhenius equation.

$$\frac{1}{(n-1)[C]^{n-1}} - \frac{1}{(n-1)[C_0]^{n-1}} = kt \quad (1)$$

where t is the residence time, k is the rate constant, n is the reaction order, C is the concentration at (t), and C_0 is the initial concentration.

An example of reaction order determination for C_7 is shown in Figure 4. The reaction order was calculated from the average of reaction orders at five different temperatures at the highest R^2 value. Table 3 shows the reaction order of each studied LMW-ME and its standard deviation. Using the obtained reaction orders, rate constants (k) were determined from Eq. (1). Based on the dependence of k with temperature, the activation energies (E_a) were obtained by plotting ln$k$ *versus* $1/T$ as shown in Figure 5. The rate constant of C_9 at 973 K was not determined because C_9 was completely decomposed at this temperature. The temperature dependence of the rate constant of C_4 was significant, and the rate constants of C_4 to C_9 gradually increased with increasing carbon number.

The standard deviations of the slopes of the regression lines and the pre-exponential factors were also calculated. Table 3 summarizes the obtained kinetic data, including reaction order ($n \pm$ SD), activation energy ($E_a \pm$ SD), and pre-exponential factor (ln$A \pm$ SD) for each LMW-ME. The reaction orders are not integer, which indicate that the decomposition of LMW-ME is complex not only involved the thermal reaction but also free radical reactions. The decomposition kinetic of soybean BDF using TGA in one-stage pyrolysis was reported by Chien *et al.* [32]. The activation

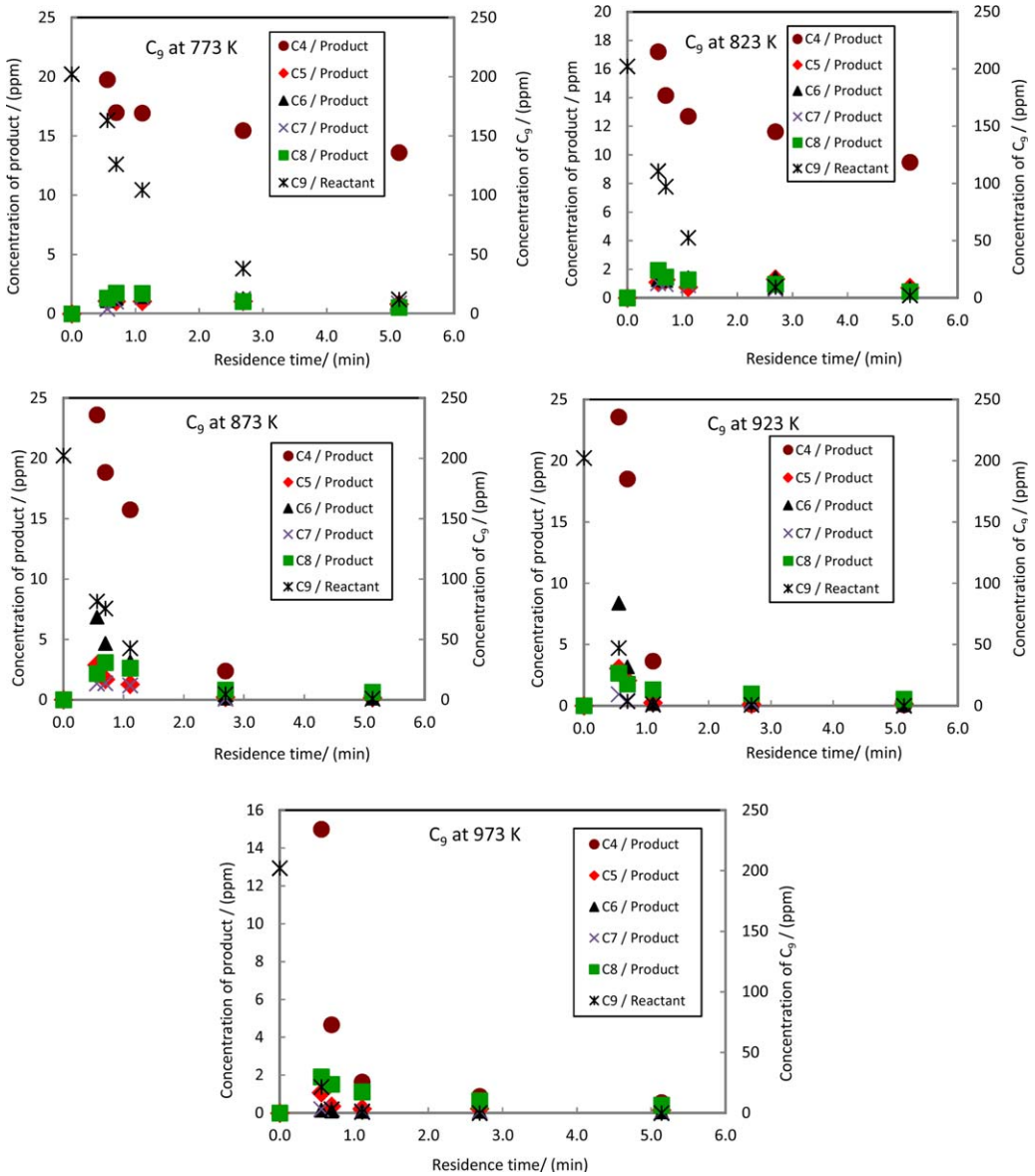

Figure 8. Decomposition of C_9 and its product formation. The left vertical-axis is the concentration of products and the right vertical-axis is the concentration of C_9. [Color figure can be viewed in the online issue, which is available at **wileyonlinelibrary.com**.]

energy and reaction order of the pyrolysis of BDF sample were 67.75 kJ mol^{-1} and 0.52, respectively. In addition, kinetic study of sunflower oil and its biodiesel were investigated. The activation energy was 50 to 75 kJ mol^{-1} and 170 to 210 kJ mol^{-1} for biodiesel and sunflower oil, respectively. With various kinetic calculation methods and fuels, the reaction order was ranged from 0.69 to 1.89 [33]. Their data are consistent with our result.

The E_a of C_4 was extremely high. E_a decreased with increasing carbon number but increased above C_8. These values may be important in further simulation studies, BDF productions and diesel engine technologies to mitigate LMW-ME emissions during biodiesel usage. Using kinetic data, the temperature-dependent decomposition rate of each LMW-ME was calculated and shown in Figure 6. Assuming the same initial concentrations, Figure 6 indicates that the decomposition of large carbon number methyl esters was faster than that of small carbon number methyl esters in the temperature range of 400 to 900 K, with the exception of C_8. The greater concentration of C_8 compared with C_7 and C_9 was due to the lower decomposition rate of C_8 compared with those of C_7 and C_9 (Figure 6). The kinetic data are consistent with previous study, where Figure 7 shows the LMW-MEs in the exhausted gas from an engine power generator using the waste cooking oil—BDF [1]. Based on the kinetic data, that explain why the concentration of C_8 in exhaust gas was higher than that of C_7 and C_9. The decomposition of C_4 was much slower than those of other MEs; therefore, C_4 was a dominant product among LMW-MEs. However, this phenomenon may be different at higher temperature because the decomposition of C_4 would be faster if the temperature reached above 1000 K. The study of the thermal decomposition of LMW-MEs at higher temperatures and shorter residence times is needed to confirm this speculation in future works.

Products of Thermal Decomposition

In the thermal decomposition of LMW-MEs, high carbon number methyl esters were cleaved into lower carbon number methyl esters. To verify the pathways of LMW-ME decomposition, LMW-MEs generated from the thermal decomposition of

each LMW-ME were determined. C_9 has the highest carbon number in the LMW-ME group. Therefore, the decomposition of individual C_9 can be observed to hypothesize the products formation. In order to investigate the reaction pathway we need more experimental data and simulation, which will be elucidated and discussed in future works. The residual reactant and by-products from the decomposition of C_9 are shown in Figure 8 while those from the decomposition of C_5 to C_8 are shows in Figures S1 to S4 in the Supporting Information, respectively. The concentration of C_4 indicated that it was an abundant product in all experiments. At both high and low temperatures, C_4 was formed immediately at a residence time of 0.29 min, before being gradually decomposed at 773 K and completely decomposed at 973 K. The concentration of C_8 was slightly greater than those of C_5, C_6, and C_7, but smaller than that of C_4. The time profile of the byproducts could not be simulated by a simple decomposition mechanism of the high carbon number methyl ester to the low carbon number methyl ester. The thermal decomposition reactions are complex, involving not only thermal reactions but also free radical reactions. To solve this problem, more experiments are needed, including many free radical reactions.

CONCLUSION

In this study, we successfully determined the detailed chemical kinetics for the thermal decomposition of LMW-MEs, which were generated by the engine combustion of BDF. The kinetic data were obtained using a continuous flow reactor system at atmospheric pressure. The significant data presented herein, including reaction orders, rate constants, and activation energies, can be widely used to predict BDF combustion in engines. Moreover, LMW-MEs are hazardous compounds that can severely affect human health and the environment. Therefore, the results of this work will be helpful in future diesel engine technologies to mitigate toxic emissions from BDF combustion. Among the LMW-MEs, the decomposition of higher carbon number esters was faster than that of smaller carbon number esters, except for C_8. C_4 was stable and abundant in the decomposition products and the rate constant increased with increasing temperature. The pathways and by-products of decomposition were hypothesized; however, further simulation is needed to clarify the mechanism of LMW-ME decomposition.

ACKNOWLEDGMENT

This research was partially supported by Japan Science and Technology Agency and Japan International Cooperation Agency, Science and Technology Research Partnership for Sustainable Development (SATREPS project entitled "Multi-beneficial measure for mitigation of climate change in Vietnam and Indochina countries by development of biomass energy").

LITERATURE CITED

1. Thang, P.Q., Maeda, Y., Trung, N.Q., & Takenaka, N. (2014). Low molecular weight methyl ester in diesel/waste cooking oil biodiesel blend exhausted gas, Fuel, 117, 1170–1171.
2. Guarieiro, L.L.N., de Souza, A.F., Torres, E.A., & de Andrade, J.B. (2009). Emission profile of 18 carbonyl compounds, CO, CO_2, and NO_x emitted by a diesel engine fuelled with diesel and ternary blends containing diesel, ethanol and biodiesel or vegetable oils, Atmospheric Environment, 43, 2754–2761.
3. He, C., Ge, Y., Tan, J., You, K., Han, X., Wang, J., You, Q., & Shah, A.N. (2009). Comparison of carbonyl compounds emissions from diesel engine fueled with biodiesel and diesel, Atmospheric Environment, 43, 3657–3661.
4. Chai, M., Lu, M., Liang, F., Tzillah, A., Dendramis, N., & Watson, L. (2013). The use of biodiesel blends on a non-road generator and its impacts on ozone formation potentials based on carbonyl emissions, Environmental Pollution, 178, 159–165.
5. Gentner, D.R., Worton, D.R., Isaacman, G., Davis, L.C., Dallmann, T.R., Wood, E.C., Herndon, S.C., Goldstein, A.H., & Harley, R.A. (2013). Chemical composition of gas-phase organic carbon emissions from motor vehicles and implications for ozone production, Environmental Science & Technology, 47, 11837–11848.
6. MSDS of LMW-ME. Available at: **http://www.sigmaaldrich.com/japan/product-catalog-jp.html**, **http://www.chemspider.com/**, **http://www.tcichemicals.com/en/ap/product/**. Accessed 14 Jan 2016.
7. Ratcliff, M.A., Dane, A.J., Williams, A., Ireland, J., Luecke, J., McCormick, R.L., & Voorhees, K.J. (2010). Diesel particle filter and fuel effects on heavy-duty diesel engine emissions, Environmental Science & Technology, 44, 8343–8349.
8. Herbinet, O., Glaude, P.A., Warth, V., & Battin-Leclerc, F. (2011). Experimental and modeling study of the thermal decomposition of methyl decanoate, Combustion and Flame, 158, 1288–1300.
9. Herbinet, O., Pitz, W.J., & Westbrook, C.K. (2008). Detailed chemical kinetic oxidation mechanism for a biodiesel surrogate, Combustion and Flame, 154, 507–528.
10. Pedersen, J.R., Ingemarsson, Å., & Olsson, J.O. (1999). Oxidation of rapeseed oil, rapeseed methyl ester (RME) and diesel fuel studied with GC/MS, Chemosphere, 38, 2467–2474.
11. Herbinet, O., Pitz, W.J., & Westbrook, C.K. (2010). Detailed chemical kinetic mechanism for the oxidation of biodiesel fuels blend surrogate, Combustion and Flame, 157, 893–908.
12. Gaïl, S., Sarathy, S.M., Thomson, M.J., Diévart, P., & Dagaut, P. (2008). Experimental and chemical kinetic modeling study of small methyl esters oxidation: Methyl (E)−2-butenoate and methyl butanoate, Combustion and Flame, 155, 635–650.
13. Westbrook, C.K., Naik, C.V., Herbinet, O., Pitz, W.J., Mehl, M., Sarathy, S.M., & Curran, H.J. (2011). Detailed chemical kinetic reaction mechanisms for soy and rapeseed biodiesel fuels, Combustion and Flame, 158, 742–755.
14. Lin, R., Zhu, Y., & Tavlarides, L.L. (2013). Mechanism and kinetics of thermal decomposition of biodiesel fuel, Fuel, 106, 593–604.
15. Diévart, P., Won, S.H., Dooley, S., Dryer, F.L., & Ju, Y. (2012). A kinetic model for methyl decanoate combustion, Combustion and Flame, 159, 1793–1805.
16. Herbinet, O., & Dayma, G. (2013). Jet-stirred reactors. In F. Battin-Leclerc, J. M. Simmie, & E. Blurock (Eds.), Cleaner combustion (pp. 183–210), London: Springer.
17. Dagaut, P., Gaïl, S., & Sahasrabudhe, M. (2007). Rapeseed oil methyl ester oxidation over extended ranges of pressure, temperature, and equivalence ratio: Experimental and modeling kinetic study, Proceedings of the Combustion Institute, 31, 2955–2961.
18. Hakka, M.H., Glaude, P.A., Herbinet, O., & Battin-Leclerc, F. (2009). Experimental study of the oxidation of large surrogates for diesel and biodiesel fuels, Combustion and Flame, 156, 2129–2144.
19. Bax, S., Hakka, M.H., Glaude, P.A., Herbinet, O., & Battin-Leclerc, F. (2010). Experimental study of the oxidation of methyl oleate in a jet-stirred reactor, Combustion and Flame, 157, 1220–1229.
20. Yang, J. & Lu, M. (2005). Thermal growth and decomposition of methylnaphthalenes, Environmental Science & Technology, 39, 3077–3082.

21. Yang, X., Felsmann, D., Kurimoto, N., Krüger, J., Wada, T., Tan, T., Carter, E.A., Kohse-Höinghaus, K., & Ju, Y. (2015). Kinetic studies of methyl acetate pyrolysis and oxidation in a flow reactor and a low-pressure flat flame using molecular-beam mass spectrometry, Proceedings of the Combustion Institute, 35, 491–498.
22. Farooq, A., Ren, W., Lam, K.Y., Davidson, D.F., Hanson, R.K., & Westbrook, C.K. (2012). Shock tube studies of methyl butanoate pyrolysis with relevance to biodiesel, Combustion and Flame, 159, 3235–3241.
23. Gauthier, B.M., Davidson, D.F., & Hanson, R.K. (2004). Shock tube determination of ignition delay times in full-blend and surrogate fuel mixtures, Combustion and Flame, 139, 300–311.
24. Jiang, X., Zhang, Y., Man, X., Pan, L., & Huang, Z. (2013). Shock tube measurements and kinetic study on ignition delay times of lean DME/n-butane blends at elevated pressures, Energy Fuel, 27, 6238–6246.
25. Jain, S. & Sharma, M.P. (2012). Application of thermogravimetric analysis for thermal stability of Jatropha curcas biodiesel, Fuel, 93, 252–257.
26. Jain, S. & Sharma, M.P. (2011). Thermal stability of biodiesel and its blends: A review, Renewable & Sustainable Energy Reviews, 15, 438–448.
27. Mukherjee, A., Das, P., & Minu, K. (2014). Thermogravimetric analysis and kinetic modelling studies of selected agro-residues and biodiesel industry wastes for pyrolytic conversion to bio-oil, Biomass Conversion and Biorefinery, 4, 259–268.
28. Mingming, L., Ming, C. (2011). Experimental investigation of the oxidation of methyl oleate: one of the major biodiesel fuel components. In Synthetic liquids production and refining (Volume 1084, pp. 289–312), American Chemical Society.
29. Norinaga, K., Janardhanan, V.M., & Deutschmann, O. (2008). Detailed chemical kinetic modeling of pyrolysis of ethylene, acetylene, and propylene at 1073–1373 K with a plug-flow reactor model, International Journal of Chemical Kinetics, 40, 199–208.
30. Yun, J.I., Kim, H.R., Kim, S.K., Kim, D., & Lee, J. (2012). Cross-metathesis of allyl halides with olefins bearing amide and ester groups, Tetrahedron, 68, 1177–1184.
31. Archambault, D. & Billaud, F. (1998). Non alimentary rapeseed oil upgrading: a parametric study of methyl oleate pyrolysis, Industiral Crops and Production, 7, 329–334.
32. Chien, Y.C., Lu, M., Chai, M., & Boreo, F.J. (2009). Characterization of biodiesel and biodiesel particulate matter by TG, TG−MS, and FTIR, Energy Fuel, 23, 202–206.
33. Santos, A.D., Caldeira, V.S., Farias, M., Araújo, A., Souza, L., & Barros, A. (2011). Characterization and kinetic study of sunflower oil and biodiesel, Journal of Thermal Analysis and Calorimetry, 106, 747–751.